Supporting information

Modulating carrier transport by cross-dimensional compositing of Ag_2Se/MXene for high-performance flexible thermoelectrics

Jie Qin[1,2,#], Yao Lu[1,#,*], Wenjing Liu[1], Zhangli Du[3], Xiang Li[1], Tianpeng Ding[3], Jianghe Feng[4], Yong Du[2,*], Qinfei Ke[2,*], Xin Wang[5,*]

[1] International School of Microelectronics, Dongguan University of Technology, Dongguan 523808, China.

[2] School of Materials Science and Engineering, Shanghai Institute of Technology, 100 Haiquan Road, Shanghai 201418, China

[3] School of Physics, University of Electronic Science and Technology of China, Chengdu 518071, China

[4] Shenzhen Institute of Advanced Electronic Materials, Shenzhen Institute of Advanced Technology, Chinese Academy of Sciences, Shenzhen 518055, China

[5] Songshan Lake Materials Laboratory, Dongguan 523808, China

# These authors contributed equally to this work.

* Corresponding authors. Email: luyao880813@126.com. ydu@sit.edu.cn.

kqf@sit.edu.cn. wangxin@sslab.org.cn.

Note 1 Experimental details

1.1 Raw materials

Ethanol (99.7%+) was obtained from General-Reagent. Ethylene glycol (EG, 98%+) was supplied by Aladdin Industrial. L-ascorbic acid (LAA, 98%), β-cyclodextrin (β-CD, 99%+), selenium dioxide (SeO_2, 99%+) were provided by Energy Chemical. Silver nitrate ($AgNO_3$, 98.5%+) was acquired from Xilong Scientific. Porous Nylon membrane with an average pore size of ~ 0.22 μm was bought from Haining DeFilter New Material Technology. Polyimide (PI) substrate was obtained from Shenzhen Office Supplies Franchise. Conductive silver paste was obtained from Guangzhou Kaixiang Electronic Products. All materials were used as received without further treatment unless otherwise indicated.

1.2 Synthesis of Se NWs

Se nanowires (NWs) were synthesized by a wet chemical method according to literature.[1, 2] SeO_2 (0.5 g) and β-CD (0.5 g) were added into 200 mL of deionized water (DI) with stirring to form Solution A. LAA (2 g) was dissolved in 200 mL of DI to form Solution B. The Solution A was slowly added to Solution B with continuous stirring. The color of the mixed solution gradually changed from colorless to yellow and eventually to brick red, indicating that amorphous selenium was formed. The reaction continued for 4 h at room temperature (RT), then the solution was centrifuged for three times in DI and ethanol alternately at 4000 rpm for 3 min to give a brick red precipitate. The precipitate was then dispersed in an appropriate amount of ethanol (400 mL) with sonication for 10 min, and then stood 24 h at RT to form flocculent precipitation Se NWs. The precipitate was collected by centrifugation at 4000 rpm for 3 min, and then re-dispersed into EG to form homogeneous dispersion for further chemical reactions.

1.3 Synthesis of Ag_2Se NWs

A certain amount of $AgNO_3$ was dissolved in 40 mL of DI with continuous stirring. Then, the $AgNO_3$ solution (the molar ratio of Ag to Se being 2:1) was added into the as-prepared EG dispersion containing Se NWs with vigorous agitation at 40 ^{o}C for 2 h. The final suspension was obtained by centrifugation for 3 times with DI and ethanol alternately at 4000 rpm for 5 min to obtain a black precipitate. The precipitate was then dried in vacuum at 60 ^{o}C for 12 h to obtain Ag_2Se NWs.

1.4 Preparation of $Mo_2TiC_2T_x$ MXene

The $Mo_2TiC_2T_x$ MXenes were prepared according to a previously reported method.[3] First, the Mo_2TiAlC_2 MAX powder was slowly added into 10 mL of HF solution (49

wt%) for etching under magnetic stirring (400 rpm) at 55 °C for 48 h. After etching, the mixture was centrifugal washed by DI water at 5000 rpm for 5 min each time until the pH of supernatant is about 6. After the last washing, the supernatant was poured out and the sediments containing multilayer $Mo_2TiC_2T_x$ MXene at the bottom of centrifuge tube were collected. Subsequently, the $Mo_2TiC_2T_x$ MXene sediments were mixed with DI water and 1 ml 25 wt% TMAOH aqueous solution at magnetic stirring of 400 rpm for 12 h for intercalation, with a sum volume of 20 ml. Then, the mixture was washed by centrifugation washing at 12000 rpm for 30 min each time to remove residual TMAOH. After two times washing, the sediments were diluted to 40 ml by DI water and the colloidal solution was bubbled using Ar for 5 min, which was subsequently sonicated at 100 W for 1 h. The sonicated mixture was centrifuged at 3500 rpm for 1 h to collect supernatant containing delaminated $Mo_2TiC_2T_x$ MXene nanosheets.

1.5 Preparation of Ag_2Se/MXene composite films

The schematic diagram of preparation of Ag_2Se/MXene composite films is shown in **Figure S1**. To ensure the consistency of film thickness, the same quality of Ag_2Se/MXene composite powders were mixed in ethanol and then sonicated at RT for 2 h to form a uniform solution (the content of MXene was from 0 to 1.5 wt%). Ag_2Se/MXene composite films were fabricated by vacuum filtration and then dried at 60 °C for 6 h under vacuum. The as-prepared films were cold-pressed at a pressure of 30 MPa for 2 min, and then hot-pressed at 10 MPa and 340 ℃ for 0.5 h under vacuum (The schematic diagram of the hot-pressing furnace is shown in the **Figure S2**). In order to determine the optimal hot-pressing temperature for Ag_2Se films, a series of hot-pressing experiments were conducted at different temperatures at a constant pressure of 10 MPa for 0.5 h (XRD was shown in **Figure S3**). The relationship between the TE performance and temperature variation was shown in **Figure S9,** where Ag_2Se films treated by hot-pressing at the temperature of x °C are named as AS_HP_ x. The results indicate that when temperature increases, both the σ and S of the TE film exhibited significant improvements. Due to the temperature limitations of the nylon substrate, some damage to the Ag_2Se film was observed after hot-pressing at 360 °C. Therefore, the optimal hot-pressing temperature was decided to 340 °C. To study the effect of the amount of MXene on the TE properties, the Ag_2Se/MXene samples with varying MXene concentration (y wt.%) after hot-pressing at 340 °C were named as MAS_y, respectively.

1.6 Assembly of f-TEGs

The Ag_2Se/MXene composite films were cut into several strips with a width of 5 mm and a length of 20 mm. A thin layer of gold electrode was deposited on both ends of the strips to reduce the contact resistance. 6 strips of the composite films were pasted on a flexible PI substrate with a spacing of 5 mm, and cooper tape was used to connect them with sliver paste in series. After being dried under vacuum at 60 °C for 6 h, the f-TEG was assembled successfully. Furthermore, TiO_2 was evenly covered on one side of the MAS to fabricate the photo-thermoelectric generator. In order to improve the efficiency, a circular f-TEG with twelve strips (5 mm × 1.25 mm) was assembled in the same method. Schematic diagram and physical drawings of the as-prepared traditional rectangle f-TEG and circular f-TEG are shown in **Figure S16**.

Note 2 Characterizations and measurements

2.1 Characterizations

The crystallinity and phase composition of the Ag_2Se NWs and films were examined by X-ray diffraction (XRD) (D8ADVACE) and X-ray photoelectron spectroscopy (XPS) (ESCALAB XI). Scanning electron microscopy (SEM) (IT500) was used to check the surface morphology of the samples. High-resolution transmission electron microscopy (HRTEM) (TALOS F200S G2) was used to observe the nanostructures of Ag_2Se/0.1wt% MXene sample. The UV-Visible-Near Infrared diffuse reflectance spectra (UV-Vis-NIR) (HATACHI UH4150) was used to characterize absorption of Ag_2Se/MXene and TiO_2-coated Ag_2Se/MXene.

2.2 Thermoelectric performance measurements

The temperature dependence of σ and S of the samples were tested by a TE test system (Cryoall CTA-3) at He atmosphere. The bending cycles dependence of R of samples was evaluated by the digital multimeter (Fluke 15B+/17B+/18B+ Multimeters). The Hall coefficient was measured by the Hall measurement system (T50, and Lake Shore 8400 Series). The in-plane thermal conductivity κ was decided by the product of the density, thermal diffusivity, and specific heat capacity ($\kappa = \rho \cdot D \cdot C_p$). The in-plane D was measured by the laser flash method (LFA467), C_p was evaluated by the differential scanning calorimetry (DSC) (DSC Q2000, TA), and the ρ was tested by measuring the mass and geometrical dimensions of the film with nylon. The output performance f-TEG were measured by a home-made apparatus (**Figure S21**), and infrared thermographic pictures of the f-TEG was taken by FTIR.

Note 3 Theoretical calculation details

3.1 single parabolic band model and Pisarenko curves

In order to further understand the thermoelectric performance of the MAS_0.1 film, the theoretical Pisarenko curves in this work were calculated using a single parabolic band (SPB) model,[4, 5] as shown in equation (1) and (2).

$$S = \frac{K_B}{e}\left(\frac{\left(\frac{5}{2}+\mathrm{r}\right)F_{\frac{3}{2}+r}(\eta)}{\left(\frac{3}{2}+r\right)F_{\frac{1}{2}+r}(\eta)} - \eta\right) \tag{1}$$

$$n_H = 4\pi\left(\frac{2m^* K_B T}{h^2}\right)^{\frac{3}{2}}\frac{F_{\frac{1}{2}}(\eta)}{R_H} \tag{2}$$

where S, K_B, e, r, h, and R_H are the Seebeck coefficient, Boltzmann constant, electron charge, scattering factor, Planck coefficient, and Hall coefficient, respectively. *Fi(η)* is the Fermi integral and η is the reduced Fermi energy. The scattering factor r = -1/2 when the acoustic phonon scattering dominants.

3.2 Thermal conductivity estimation

In the TPET techniques,[6] the MAS_0.1 film was suspended between two copper or aluminum electrodes using silver paste and a step laser beam was used to heat the sample. The thermal diffusivity (α) can be calculated by the equation (3) as follow:

$$\alpha = \alpha_{con} + \alpha_{cov} + \alpha_{rad} = \alpha_{con} + \frac{1}{\rho C_p D}\left(\frac{2h}{\pi^2} + \frac{8\xi\sigma T^3}{\pi^2}\right) \times L^2 \tag{3}$$

where α, α_{con}, α_{cov}, and α_{rad} is the measured thermal diffusivity, real thermal diffusivity, heat convection, and heat radiation, respectively. ρ is the density, C_p is the specific heat, h is heat convection coefficient, ξ is the emissivity, σ is the Stephen-Boltzmann constant, T is absolute temperature, and D is the thickness of the sample, respectively. As illustrated in equation (3), if the other parameters are kept constant, the α is linearly proportional to L^2. Thus, the real thermal diffusivity α_{con} can be accurately obtained by linearly fitting using different lengths of sample measurements (**Figure S13b**). Thus, the real thermal conductivity of the MAS_0.1 film can be calculated to be 0.48 W/mK by equation (4):

$$\kappa = \rho C_p \alpha \tag{4}$$

We estimated the thermal conductivity using series-parallel connected model, respectively, using the following formulas:[7]

$$\kappa_p = \kappa_{Ag_2Se} \times v_{Ag_2Se} + \kappa_{MXene} \times v_{MXene} \quad (5)$$

$$\frac{1}{\kappa_s} = \frac{v_{Ag_2Se}}{\kappa_{Ag_2Se}} + \frac{v_{MXene}}{\kappa_{MXene}} \quad (6)$$

where κ_{Ag_2Se} and κ_{MXene} are the thermal conductivity of bulk Ag_2Se and MXene, and chosen as 0.6-1.0 W/mK,[7-9] and 0.15 W/mK,[10] respectively; v_{Ag_2Se} and v_{MXene} are the volume fraction of Ag_2Se and MXene, estimated to be 0.75 and 0.05 (porosity ~ 20%) from SEM and TEM observations. The corresponding κ_p and κ_s are 0.46-0.76, 0.63-0.92 W/mK, respectively.

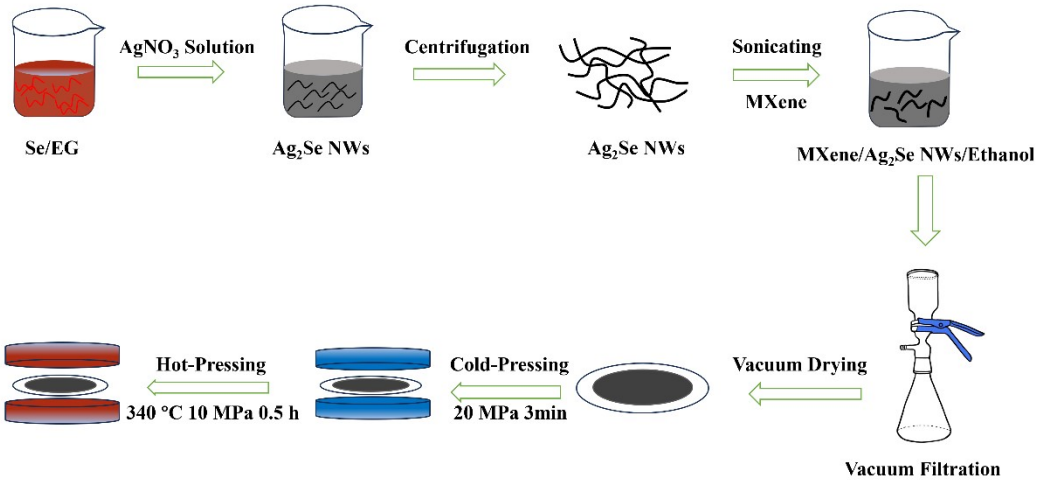

Figure S1. Schematic diagram of preparation of Ag_2Se/MXene composite films.

Figure S2. Schematic diagram of the thermocouple location in a vacuum tube high-temperature sintering furnace.

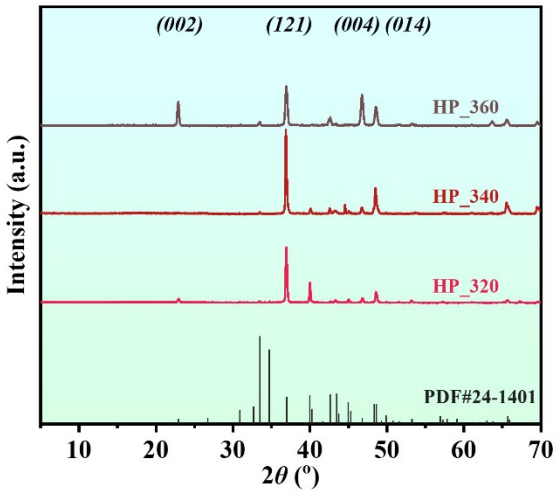

Figure S3. XRD diffractograms of as-prepared Ag_2Se films after hot pressing at different temperatures (320 °C, 340 °C, and 360 °C).

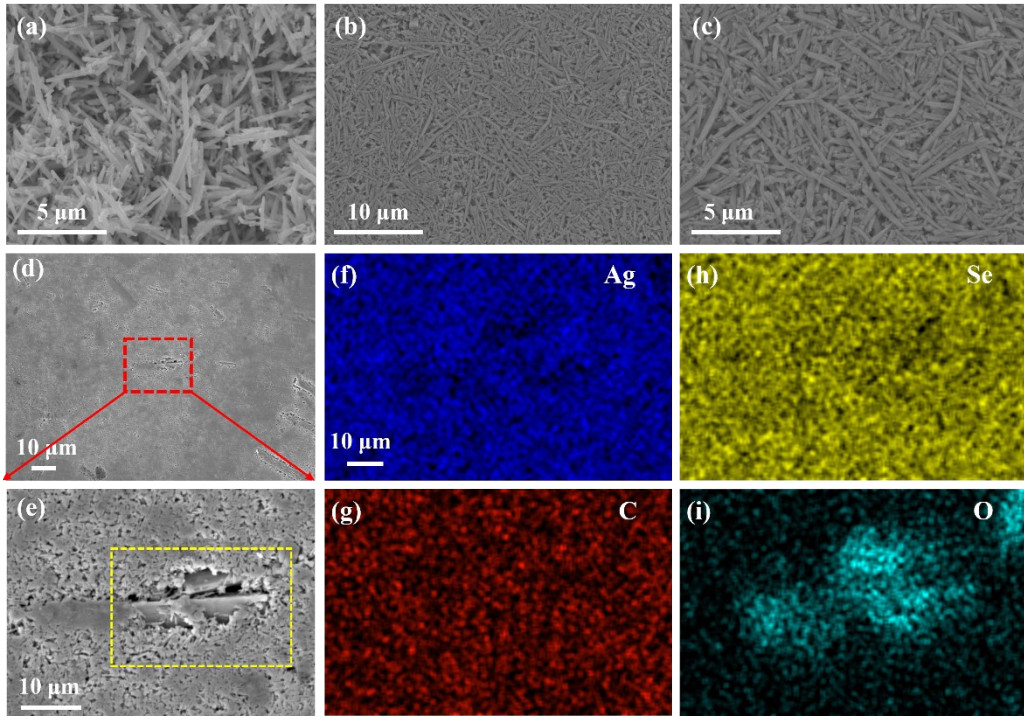

Figure S4. Typical SEM surface images of Ag_2Se/MXene (0.1 wt%) composite film before cold-pressing (a), after cold-pressing (b & c), and after hot-pressing (d & e). Corresponding EDS mapping of (f) Ag element, (g) C element, (h) Se element, (i) O element.

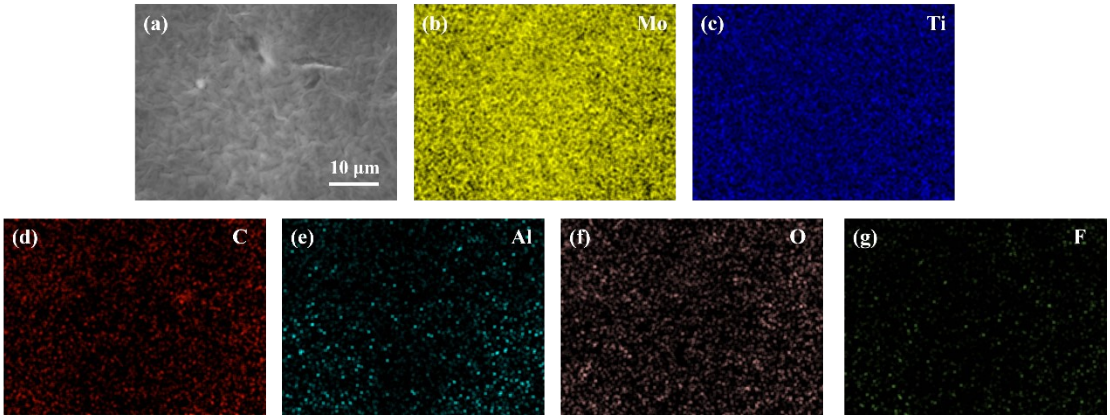

Figure S5. (a) SEM image of MXene film. EDS maps showing elements of (b) Mo, (c) Ti, (d) C, (e) Al, (f) O, and (g) F.

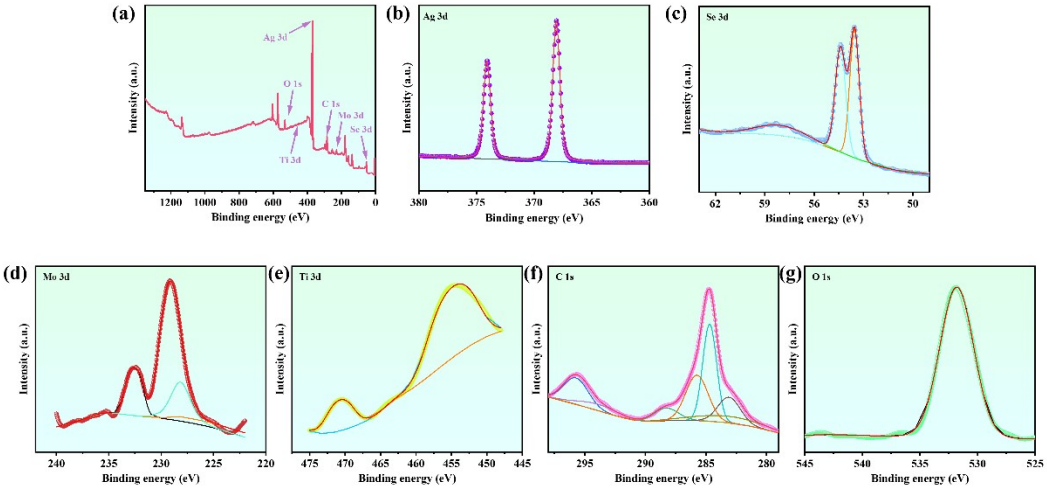

Figure S6. XPS analysis of the MAS_0.1 film: (a) XPS survey spectrum, (b) Ag_3d, (c) Se_3d, (d) Mo_3d, (e) Ti_3d, (f) C_1s, and (g) O_1s.

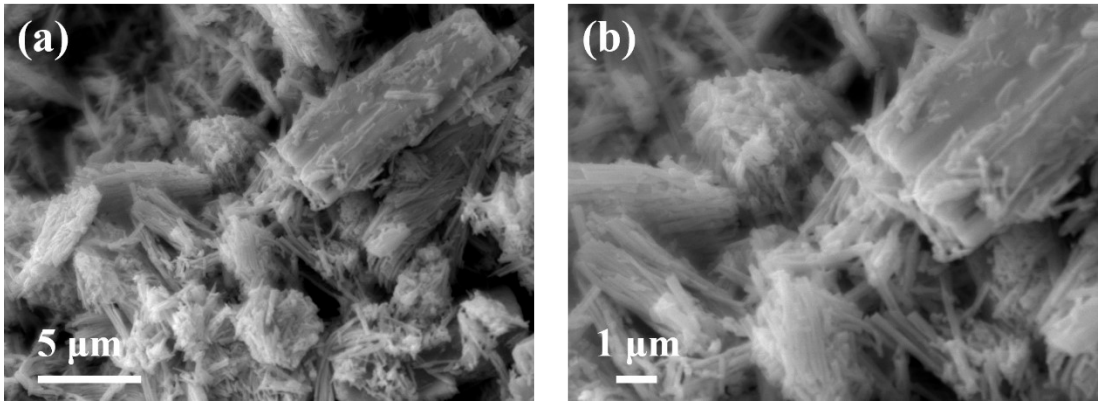

Figure S7. Typical surface SEM images of the Ag_2Se/MXene composites at (a) low and (b) high magnification.

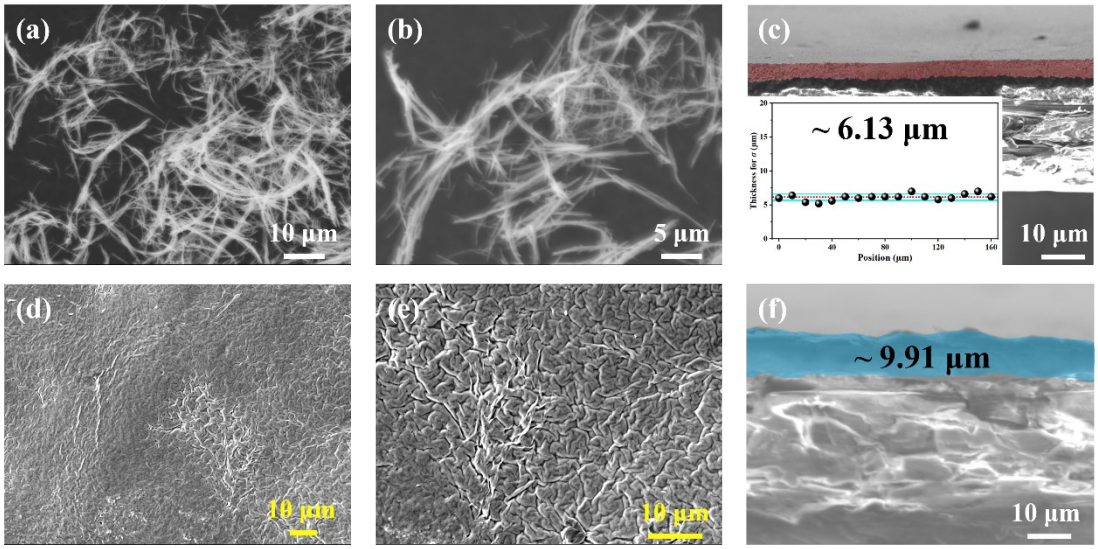

Figure S8. Typical surface SEM images of the Ag_2Se powder at (a) low and (b) high magnification. (c) Fractured surface SEM image of the hot-pressed Ag_2Se/MXene film. Typical surface SEM images of the hot-pressed MXene film at (d) low, (e) high magnification. (f) Fractured surface SEM image of the MXene film.

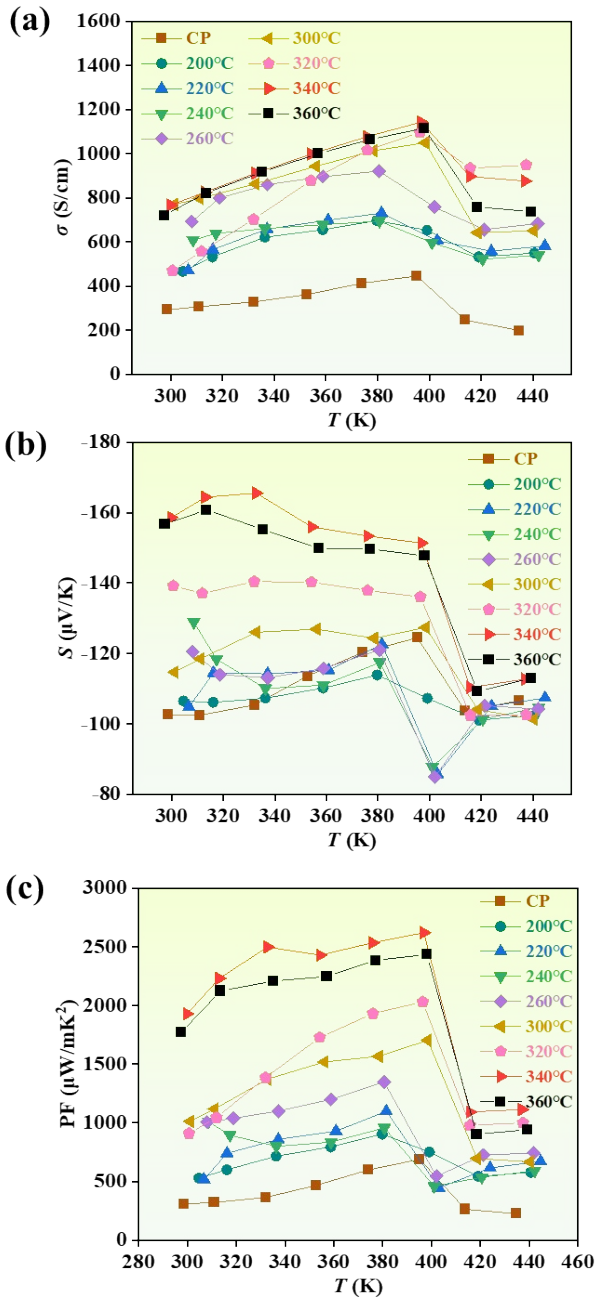

Figure S9. Temperature dependence of (a) σ, (b) S, and (c) PF of Ag_2Se films at different hot-pressing temperatures.

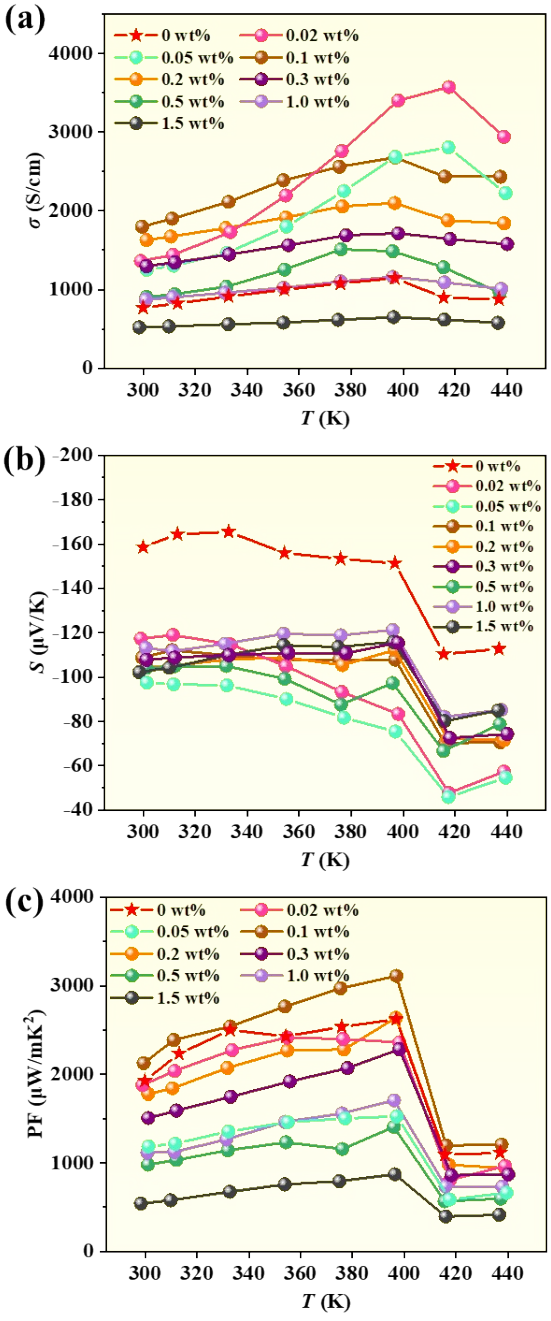

Figure S10. Temperature dependence of (a) σ, (b) S, and (c) PF of Ag_2Se/MXene films with various MXene concentration after hot-pressing at 340 °C.

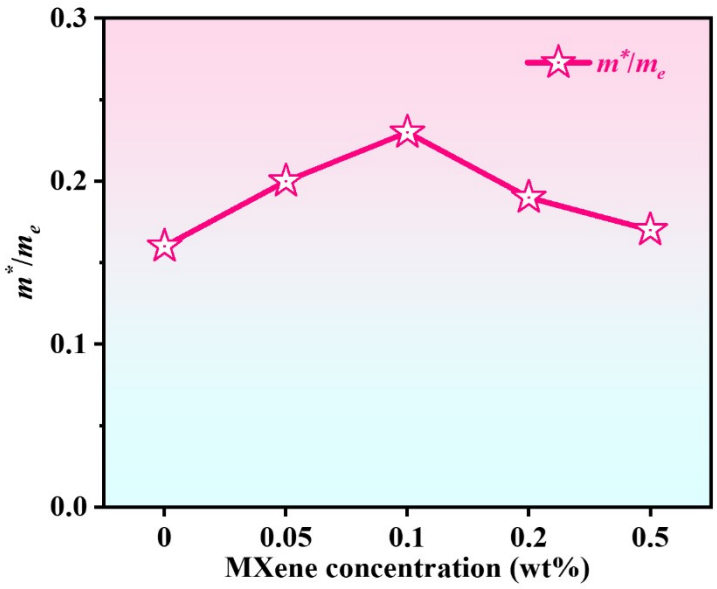

Figure S11. m^*/m_e of the composites as a function of MXene concentration based on SPB model.

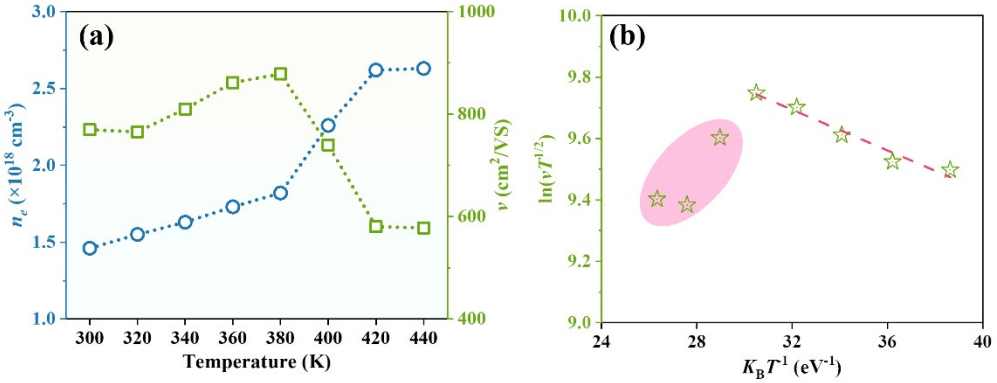

Figure S12. (a) Temperature dependence of n and v, and (b) corresponding ln($vT^{1/2}$) as a function of K_BT^{-1} of the MAS_0.1 film.

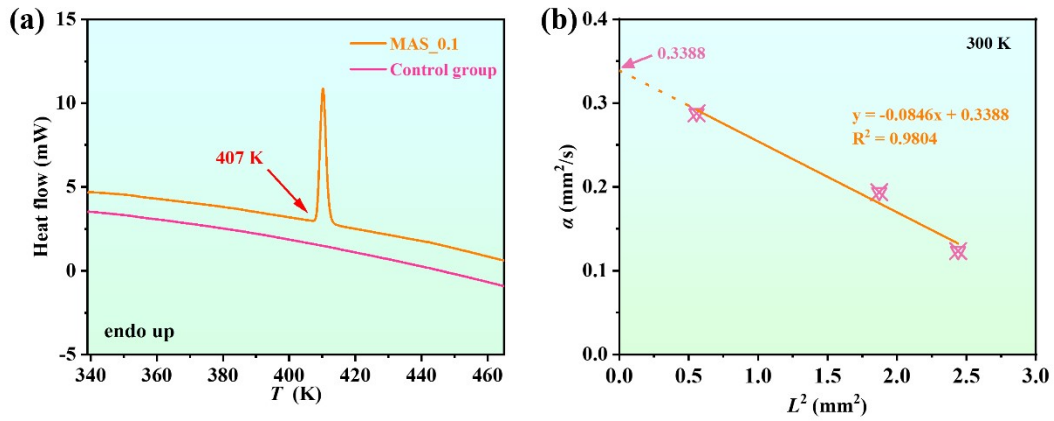

Figure S13. (a) Heat flow versus temperature of the MAS_0.1 film, and (b) linear fit of α - L^2 for the MAS_0.1 film.

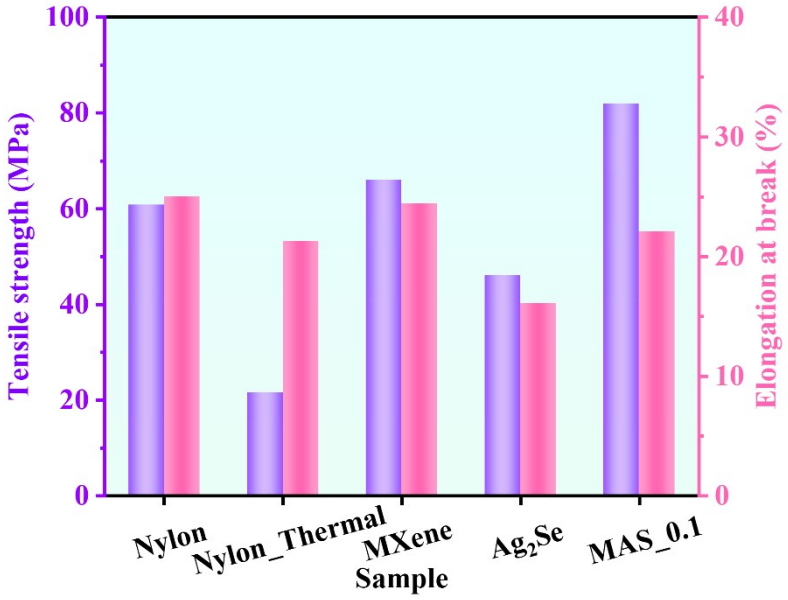

Figure S14. Tensile strength and elongation at break of nylon membrane, nylon_thermal film, MXene film, Ag_2Se film, and MAS_0.1 film.

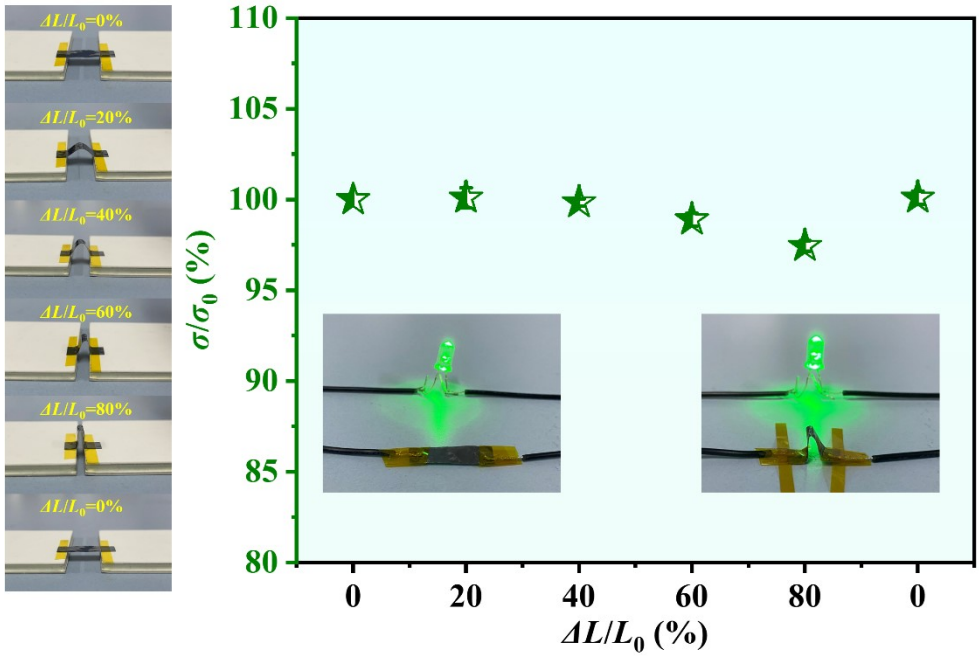

Figure S15. Digital photographs of MAS_0.1 film under various compression states along with the corresponding changes in σ/σ_0 with varying $\Delta L/L_0$. The inset showcases the illumination of a LED in an electric circuit connected by MAS_0.1 film at different compression states.

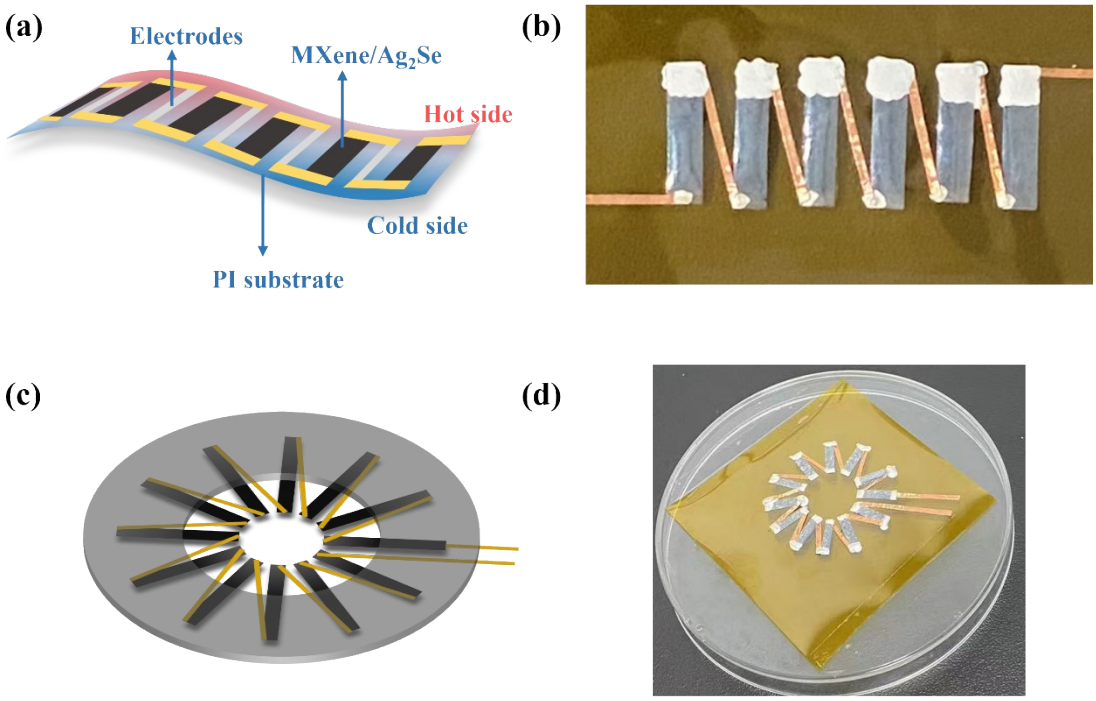

Figure S16. Schematic diagram and physical drawings of the as-prepared traditional rectangle f-TEG (a, b) and circular f-TEG (c, d).

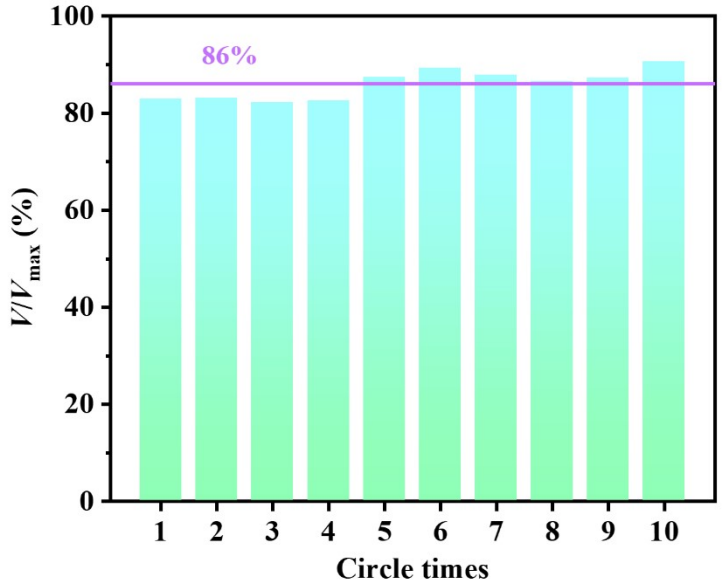

Figure S17. Response efficiency ($V_{oc\text{-}1s}/V_{oc\text{-}max}$) of the rectangle f-TEG reaching ~ 86% within 1 s from 10 trials.

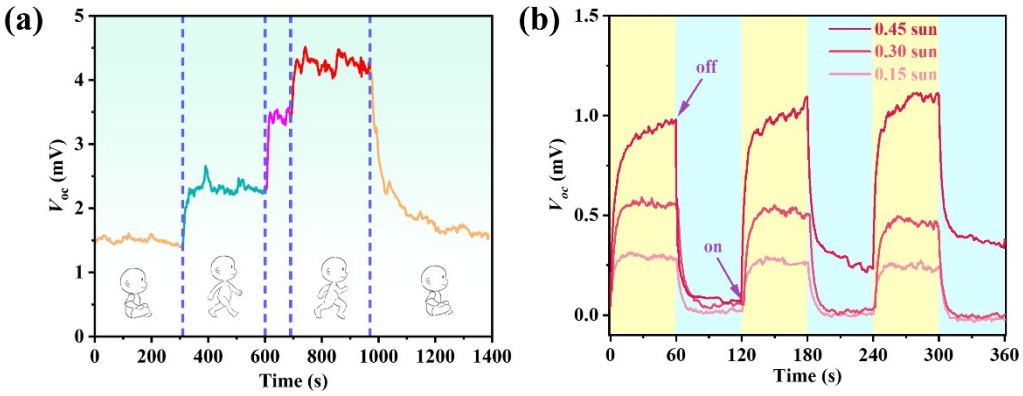

Figure S18. (a) The relationship between open circuit voltage of f-TEG and time in response to different body movements (sitting, walking, running). (b) Change between open circuit voltage and time when exposed to light of varying intensities.

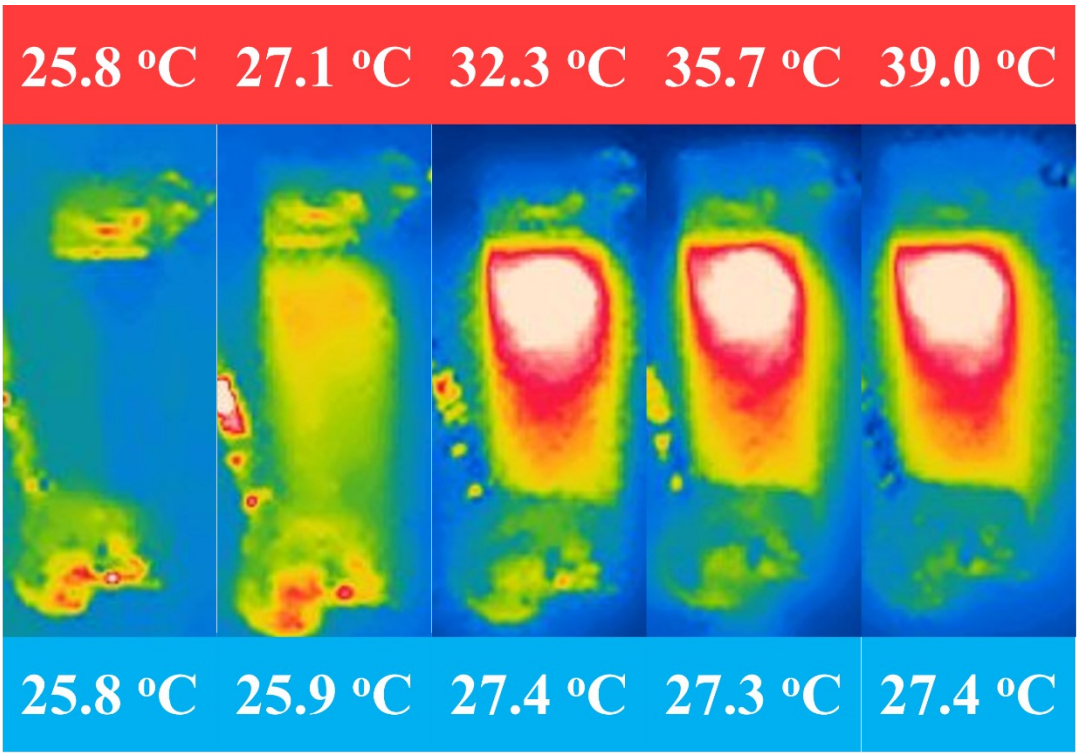

Figure S19. Infrared thermal images showing the temperature differences of MAS_0.1 film after applying different currents.

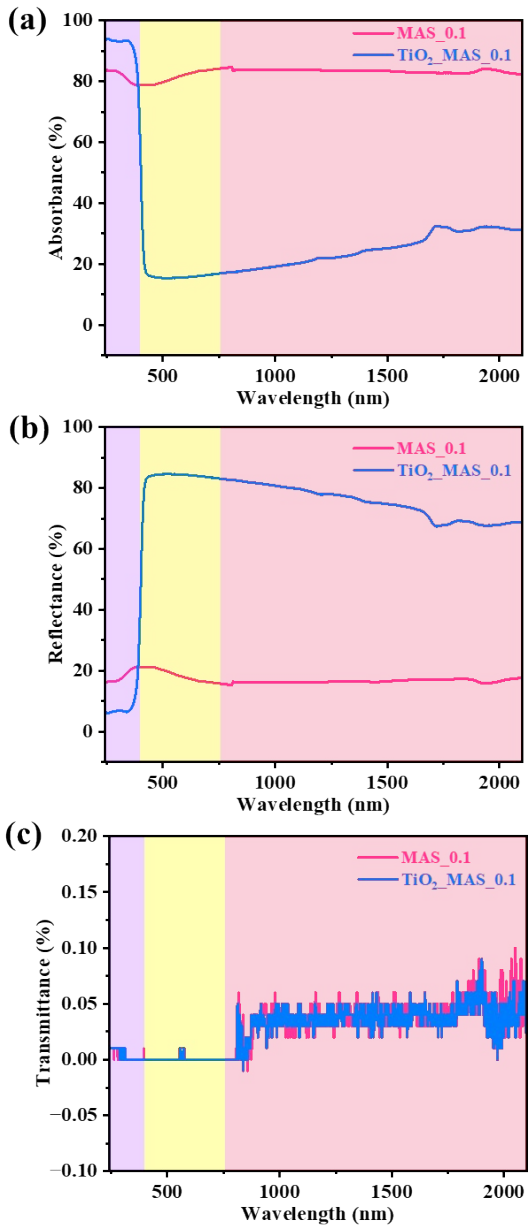

Figure S20. (a) Absorbance, (b) reflectance, and (c) transmittance of MAS_0.1 film and TiO_2_MAS_0.1 film in the solar radiation spectrum. The visible light range is highlighted in yellow.

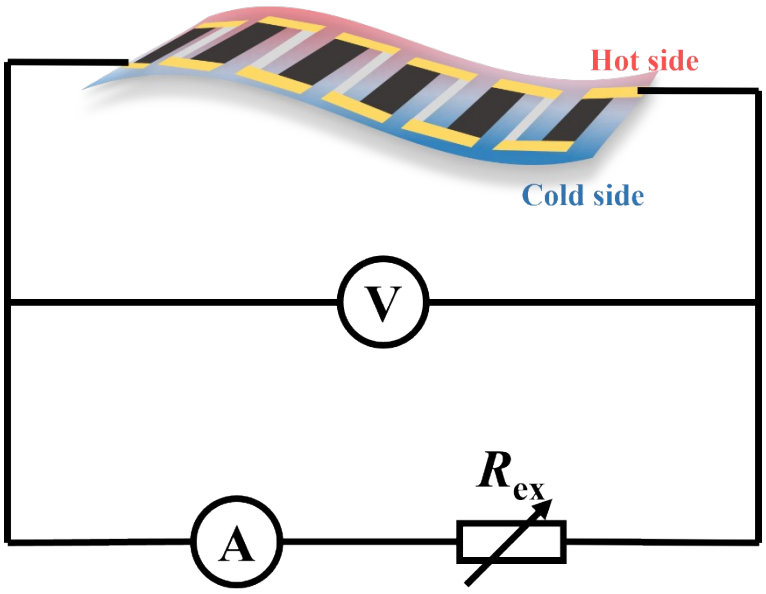

Figure S21. Schematic diagram for output performance measurement of the f-TEG.

Table S1. Details of thermal property of MAS_0.1 film

Temperature (K)	Density (g/cm^3)	Thermal diffusivity (mm^2/s)	Specific heat capacity (J/gK)	Thermal conductivity (W/mK)
300	1.67	0.34	0.84	0.48

Reference

1. Y. Ding, Y. Qiu, K. Cai, Q. Yao, S. Chen, L. Chen and J. He, *Nat. Commun.*, 2019, **10**, 841.
2. Y. Lu, Y. Qiu, K. Cai, Y. Ding, M. Wang, C. Jiang, Q. Yao, C. Huang, L. Chen and J. He, *Energy Environ. Sci.*, 2020, **13**, 1240-1249.
3. L. Chang, T. Zhang, F. Wang, H. Ma, W. Xie, T. Ding and X. Xiao, *2D Mater.*, 2022, **10**, 014009.
4. Q.-X. Hu, W.-D. Liu, L. Zhang, W. Sun, H. Gao, X.-L. Shi, Y.-L. Yang, Q. Liu and Z.-G. Chen, *Chem. Eng. J.*, 2023, **457**, 141024.
5. P. Wang, J.-L. Chen, Q. Zhou, Y. T. Liao, Y. Peng, J. S. Liang and L. Miao, *Appl. Phys. Lett.*, 2022, **120**, 193902.
6. Y. Ling, M. Han, J. Xie, G. Qiu, G. Dong, E. Min, P. Zhang, X. Zeng, R. Liu and R. Sun, *Measurement*, 2023, **217**, 113058.
7. Y. Li, Q. Lou, J. Yang, K. Cai, Y. Liu, Y. Lu, Y. Qiu, Y. Lu, Z. Wang, M. Wu, J. He and S. Shen, *Adv. Funct. Mater.*, 2021, **32**, 2106902.
8. Y. Lu, Y. Qiu, K. Cai, X. Li, M. Gao, C. Jiang and J. He, *Mater. Today Phys.*, 2020, **14**, 100223.
9. C. Jiang, P. Wei, Y. Ding, K. Cai, L. Tong, Q. Gao, Y. Lu, W. Zhao and S. Chen, *Nano Energy*, 2021, **80**, 105488.
10. L. Yu, L. Xu, L. Lu, Z. Alhalili and X. Zhou, *Chemphyschem*, 2022, **23**, 202200203.